Tensile Buckling of Advanced Turboprops

C. C. Chamis* and R. A. Aiello†
NASA Lewis Research Center, Cleveland, Ohio

Theoretical studies were conducted to determine analytically the tensile buckling of advanced propeller blades (turboprops) in centrifugal fields, as well as the effects of tensile buckling on resonant frequencies. Theoretical studies were also conducted to establish the advantages of using "high-performance" composite turboprops as compared to titanium. Results show that the vibration frequencies are not affected appreciably prior to 80% of the tensile buckling speed. Some frequencies approach zero as the tensile buckling speed is approached. Composites provide a substantial advantage over titanium on a buckling speed-to-weight basis. Vibration modes change as the rotor speed is increased and substantial geometric coupling is present.

Introduction

THE use of thin, highly swept, and twisted propeller blades (turboprops) is important to the development of efficient and quiet advanced aircraft (Fig. 1). The high sweep angle (as high as 60 deg for the turboprop reported herein) produces a significant reduction in noise and is, therefore, a desirable design feature. However, blades of this type (thin, highly swept, twisted) exhibit a complex state of structural response under a centrifugal force field requiring special analysis techniques.[1] These techniques are required to establish the rotor speed regions of various instabilities, including tensile buckling. The objective of this paper is to describe theoretical studies that were performed at NASA Lewis to determine analytically the tensile buckling of advanced titanium turboprops in centrifugal force fields, as well as the effects of tensile buckling on other types of structural behavior, such as resonant frequencies and flutter. Another objective of the paper is to identify any advantages of using "high-performance" composite turboprops in order to change the regions of instability. The theoretical studies were performed using an in-house program designed for composite blade analysis. The turboprop geometry and material used, tensile buckling mechanisms (physics), tensile buckling predictions, and tensile buckling effects on frequencies are described in detail, including geometric and material coupling.

Turboprop Description

The simulated turboprop blade (propeller) used in the analysis is shown in Fig. 1. It is about 10 in. long and has a tip chord of 2 in. and a maximum chord at the hump of about 3.5 in. Thickness varies from 1 in. at midchord at the root to 0.040 in. at midchord at the tip. The leading-edge thickness varies from 0.180 in. at the root to 0.022 in. at the tip. The trailing-edge thickness varies from 0.077 in. at the root to 0.016 in. at the tip. The turboprop has a twist of 33.2 deg and tip sweep angle of 60 deg. The turboprop finite element analysis model is shown in Fig. 2. This model consists of 423 grid points and 744 CTRIA2 elements. The number of unrestrained degrees of freedom is 2466. First, a turboprop made from titanium was analyzed. Second, the titanium was replaced with high-performance composites to determine the advantages of composites on the tensile buckling and the other instabilities. The high-performance composite was assumed to be type AS graphite-fiber/epoxy matrix at about 60% fiber by volume. Stiff ±45 deg plies were assumed to be made with fibers having 75×10^6 psi modulus in order to study the shear stiffening effects.

Tensile Buckling: Mechanisms

Tensile buckling occurs in swept turboprops because a compression-stress region develops at the hump (Fig. 3) under a centrifugal force field. The magnitude of the compression force in this region grows as the rotor speed is increased. Simultaneously, the boundary of the compression region grows because of the progressive change in the spatial position of the turboprop. This progressive change in spatial position produces changes in the direction and magnitude of the relative centrifugal acceleration and consequently changes in the centrifugal field. This region grows from the leading edge toward the center and along the span as the rotor speed is increased. The compression-stress region growth shown in Fig. 3 is for a simulated 60 deg swept titanium turboprop as the rotor speed increases from 1500 to 9000 rpm and accounting for spatial position changes.[1] The compression-stress region growth is greater along the span toward the tip than it is toward the center of the airfoil or toward the root.

As the rotor speed is increased, the compression-stress region continues to grow to a critical size at which elastic instability (buckling) is incipient. This structural instability is identified herein as tensile buckling because it is induced by a tensile centrifugal force field. The corresponding rotor speed is identified as the tensile buckling rotor speed.

Tensile buckling of swept turboprops is analogous to the buckling of plates subjected to in-plane bending (see Ref. 2 for isotropic plates and Ref. 3 for anisotropic plates). The in-plane bending in the hump region is induced by the swept portion of the turboprop because this portion tends to straighten out as the centrifugal force increases. The twist and the helical stacking axis also contribute to in-plane bending. For example, the elemental vector equations for relative force and moment induced by an element (ξ, η, ζ) outboard of the hump on an element (x, y, z) at the hump are, respectively (see Fig. 4a),

$$\Delta F=\Delta m\Omega_z^2[(\xi-x)i+(\eta-y)j] \tag{1}$$

$$\Delta M=\Delta m\Omega_z^2[(\xi-x)(\eta-y)k+(\zeta-z)(\xi-x)j - (\zeta-z)(\eta-y)i] \tag{2}$$

where Δm is the elemental mass at (ξ, η, ζ) Ω_z the rotor speed, and (i, j, k) are unit vectors corresponding to (x, y, z).

Presented as AIAA Paper 82-0776 at the 23rd AIAA/ASME/ASCE/AHS 23rd Structures, Structural Dynamics and Materials Conference, New Orleans, La., May 10-12, 1982; submitted July 2, 1982; revision received June 7, 1983.

*Aerospace Structures and Composites Specialist. Associate Fellow AIAA.
†Aerospace Engineer.

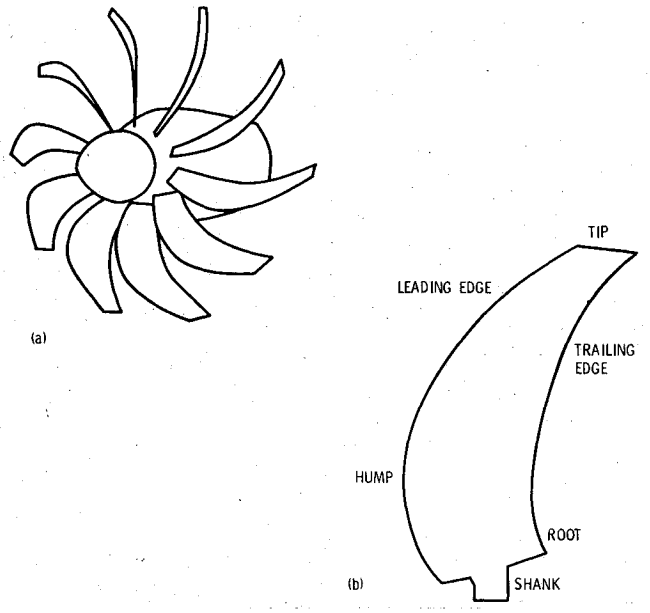

Fig. 1 Turboprop stage and propeller blade (turboprop): a) stage, b) propeller blade (turboprop).

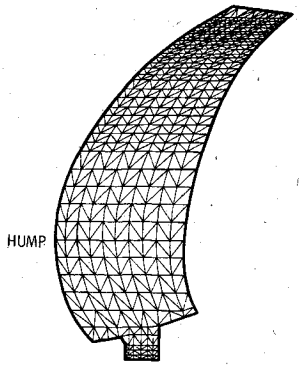

Fig. 2 Turboprop propeller finite element model (423 grid points, 744 elements).

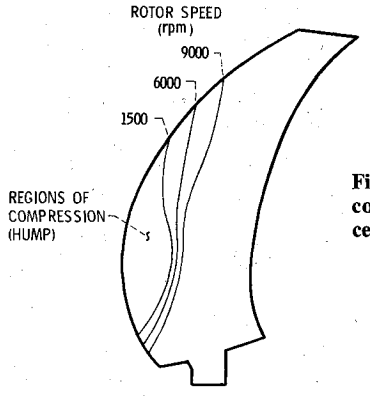

Fig. 3 Turboprop propeller compression regions from centrifugal force field.

Two interesting points can be identified in Eqs. (1) and (2). First, any element outboard of the hump will induce a radial and a tangential force at the hump element. Second, the outboard element will induce three moments at the hump element: an in-plane moment k, an out of plane moment j, and a twisting moment i. These moments induce one in-plane normal force, one in-plane shear, and one through-the-thickness shear. The integrated forces and moments of all elements outboard of (x, y, z) can be determined by integrating Eqs. (1) and (2) as (ξ, η, ζ) varies from (x, y, z) to the tip of the turboprop. This integration is complex and not easily amenable to closed-form integration. However, the variation of the forces and moments across the chord through (x, y, z) can readily be obtained using finite element analysis. For example, the force variation results for a special case (titanium turboprop, 6000 rpm, chord section at 5.5 in radius) is shown in Fig. 4b. As can be seen, the in-plane compression force F_x at the leading edge is substantial as is the in-plane shear F_z. Also, the variation of all the forces (F_x, F_y, F_z) across the chord is nonlinear.

Equations (1) and (2) can be combined to illustrate the analogy between the tensile buckling of a turboprop and a plate in in-plane bending. This is accomplished by assuming that the turboprop is a plate of uniform thickness and lies in the $(x\text{-}y)$ plane (Fig. 4a). The resulting elemental equation is

$$\Delta N = \frac{\Delta m \Omega_z^2}{C} (\xi - x) \left[1 - \frac{12y}{C^2} (\eta - y) \right] \tag{3}$$

where N is the in-plane force per unit chord and C the chord width at the hump through (x, y). The first term in the brackets is due to in-plane force while the second is due to in-plane bending. Equation (3) is analogous to those described in Refs. 2 and 3. Equation (3) shows that the compression field is a function of spatial position and *not* of the rotational speed when the rotational speed is applied only in the initial turboprop position, that is, where geometric nonlinearities are neglected.

Tensile Buckling: Prediction

The tensile buckling of the swept turboprops was predicted using COBSTRAN (composite blade structural analysis). COBSTRAN consists of composite mechanics, a blade finite element generator, and NASTRAN.[4] Turboprops made from isotropic materials are handled as special cases in COBSTRAN. Since NASTRAN is a part of COBSTRAN, tensile buckling was predicted by using the NASTRAN Rigid FORMAT 5. Rigid FORMAT 5 predicts buckling, in general, using the differential stiffness methods.[5] The loading conditions, boundary conditions, and solution methods are user-supplied information within COBSTRAN, which merges them with the NASTRAN bulk data prior to calling NASTRAN.

The procedure used for determining the rotor speed that will induce tensile buckling in turboprops is as follows:

1) Run COBSTRAN with a selected rotor speed (1500 rpm was used for the first speed).

2) Examine the eigenvalue. Two cases are possible: a) negative eigenvalue indicating *no* tensile buckling is possible under this selected mode; or b) positive eigenvalue indicating the tensile buckling mode selected is possible.

3) If the eigenvalue is negative, increase the rotor speed and/or select a different mode, and run COBSTRAN again. The different mode is selected by specifying different eigenvalue ranges.

4) If the eigenvalue is positive, determine the rotor speed (Ω_{zcr}) inducing tensile buckling from

$$\Omega_{zcr} = \sqrt{\lambda^2} \Omega_z \tag{4}$$

where Ω_z is the rotor speed used and λ^2 the eigenvalue predicted by NASTRAN.

5) Check Ω_{zcr} with at least two additional values of progressively greater rotor speeds Ω to ascertain that the tensile buckling mode is the lowest mode represented by a positive eigenvalue.

Rotor speeds Ω_{zcr} inducing tensile buckling in the 60 deg swept titanium and composite turboprops are summarized in Table 1. In addition, an unswept composite turboprop and a swept turboprop with stiff ± 45 deg plies are included. The unswept turboprop is included to show that it does not have a possible tensile buckling mode. The swept turboprop with the stiff ± 45 deg plies is included to illustrate increased shear-stiffness effect on tensile buckling speeds. The stiff ± 45 deg plies were assumed to be made from a composite with a

Table 1 Summary of tensile buckling speeds

Turboprop	Rotor speed (rpm) at tensile buckling
Unswept—composite	N/A
Swept—titanium	12,470
Swept—composite	10,950
Swept—composite (stiff ±45 plies)	11,370

NOTE: N/A—not applicable (unswept turboprops are not subject to tensile buckling).

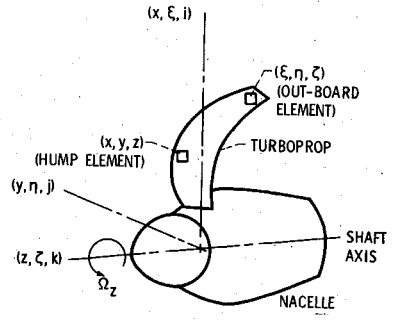

a) geometry schematic

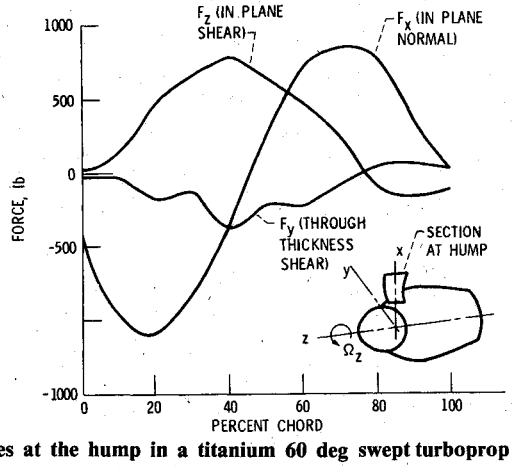

b) forces at the hump in a titanium 60 deg swept turboprop ($x = 5.5$ in., $\Omega_z = 6000$ rpm.)

Fig. 4 Schematic depicting source of compression forces in the hump region of swept turboprop.

graphite fiber having a 75×10^6 psi modulus. The fiber modulus used in the other composites was assumed to be 32×10^6 psi. All composite properties needed are generated within COBSTRAN.

It can be seen in Table 1 that 1) the titanium turboprop has about 15% higher tensile buckling rotor speeds than the composite, and 2) increased shear stiffness has negligible effects on the tensile buckling speed of composite turboprops.

The increased tensile buckling speed for the titanium turboprop is attributed, in part, to combinations of higher chordwise and shear stiffness of the titanium compared to composite, even though the density of the composite is less. However, on the basis of rotor speed to density (same airfoil volume for both), the tensile buckling speed for the composite turboprop is 182,500 rpm/lb compared to 77,940 rpm/lb for the titanium. This value translates to a 134% advantage for the tensile buckling speed of the composite turboprop over the titanium. The conclusion from this discussion is that composite turboprops have a substantial weight advantage over titanium for the same tensile buckling speed.

The lowest tensile buckling modes for both turboprops are shown in Fig. 5. The modes are about the same for both turboprops. The modes are primarily tip modes and are highly coupled since the out-of-plane and the in-plane displacements

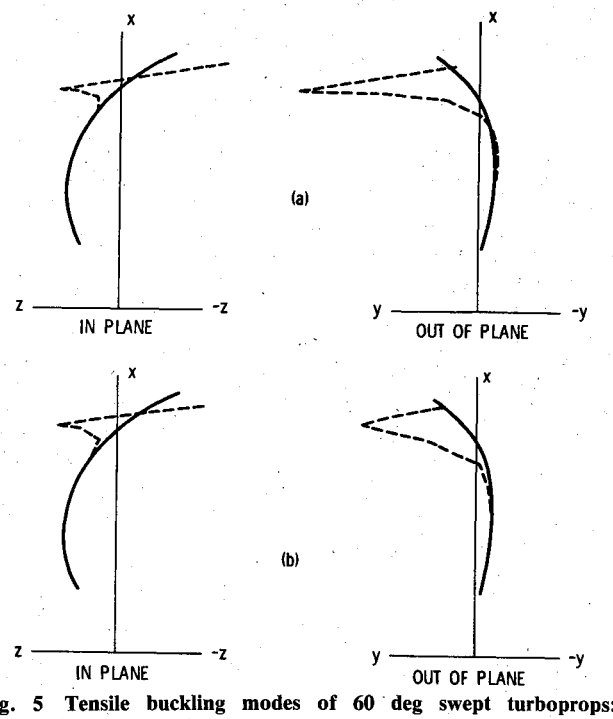

Fig. 5 Tensile buckling modes of 60 deg swept turboprops: a) titanium, b) composite.

have about the same magnitude. This discussion leads to the conclusion that rotor speeds which induce tensile buckling in swept turboprops can be determined from the procedures described herein.

Tensile Buckling Effects on Frequencies

Tensile buckling effects on vibration frequencies of swept turboprops are similar to those of a compressive load on the frequencies of a structural component. For example, the equation of the lowest frequency of a vibrating beam subjected to a compressive load is given by[6]

$$\omega = \frac{\alpha \pi^2}{\ell} \left(\frac{EI}{M}\right)^{1/2} \left[1 - \frac{N}{N_{cr}}\right]^{1/2} \tag{5}$$

where ω is the lowest frequency, α a constant depending on the boundary conditions, ℓ the length, EI the bending stiffness, m the mass per unit length, N the compressive force, and N_{cr} the buckling load. The important point to be noted in Eq. (5) is that the frequency decreases as N/N_{cr} increases and is zero where N equals N_{cr}. The reduction in the vibration frequencies of the swept turboprops is not as severe as indicated in Eq. (5). The reason is that the in-plane force F_x induced by the centrifugal force field is not uniform, but varies as shown in Fig. 4b.

The vibration effects on the variation of the forces and moments can be illustrated by perturbing Eqs. (1) and (2) about an equilibrium steady-state position with displacement fields (U_ξ, V_η, W_ζ) at (ξ, η, ζ) and with (U_x, V_y, W_z) at (x, y, z); see Fig. 4a. The resulting equations are given by

$$\Delta F = \Delta m \Omega_z^2 \{ [\xi - x + u_f - u_x] i + [\eta - y + v_\eta - v_y] j \} \tag{6}$$

$$\begin{aligned} \Delta M = \Delta m L_z^2 \{ & [(z-x)(\eta-y) + (u_\xi - u_x)(\eta-y) \\ & + (u_\xi - u_x)(v_\eta - v_y)] k + [(\zeta - z)(\xi - x) \\ & + (w_\zeta - w_z)(\xi - x) + (w_\zeta - w_z)(u_\xi - u_x)] j \\ & - [(\zeta - z)(\eta - y) + (w_\zeta - w_z)(\eta - y) \\ & + (w_\zeta - w_z)(v_\eta - v_y)] i \} \end{aligned} \tag{7}$$

It can be seen in both Eqs. (6) and (7) that the changes in both force and moment can be stabilizing or destabilizing, depending on the signs of the respective displacements u_ξ and u_x, etc. Note the nonlinear geometric effects of displacement products $(u_\xi - u_x)(v_\eta - v_y)$, etc., on the elemental moment. The contribution of these geometric nonlinear effects depends on the magnitudes and signs of the displacements. Since the lowest vibration mode is similar to the buckling mode, it can be seen in Fig. 5 that the displacements are substantial at the tip but relatively small at the hump.

The effects of possible tensile buckling on the frequencies of swept turboprops were predicted using COBSTRAN. The procedure used is that available in NASTRAN through Rigid FORMAT 13. The differential stiffness with appropriate eigenvalue extraction routines are used to calculate vibration frequencies and mode shapes of structural components in centrifugal force fields (geometric stiffening). The procedure used in NASTRAN for calculating vibration frequencies is similar to that used for calculating buckling described previously. The frequencies predicted are summarized in Table 2 for the titanium turboprop and in Table 3 for the composite.

The effects of possible tensile buckling on the vibration frequencies are best illustrated on an interference frequency vs rotor speed (Campbell) diagram. Results for the 60 deg swept composite turboprop are shown in Fig. 6. The frequencies (except the second) decrease as the tensile buckling rotor speed is approached. The first frequency is decreasing very rapidly and will be zero at the tensile buckling rotor speed. In contrast, the frequencies increase or remain about the same (second vibration mode, for example) with increasing rotor speed in the absence of compression force regions. One important observation in Fig. 6 is that no appreciable reduction in frequencies occurs prior to about 80% of the tensile buckling rotor speed.

The interference of vibration frequencies with rotor excitation orders [such as one per revolution (1E), two per revolution (2E), etc.] are important in actual design practice. The influence of tensile buckling on frequencies at operational conditions can be illustrated by assuming a 7500 rpm design rotor speed with $\pm 10\%$ margins (Fig. 6). It is worth noting that the 5E engine excitation is the only one, and only slightly, within the operating margins of the fourth vibration mode frequency. It can also be seen that the margin between operating speed and tensile buckling is substantial.

The vibration mode shapes are of interest because they show graphically the areas of predominant motion. The effects of rotor speed on the mode 1 vibration are shown in Fig. 7 for four different rotor speeds. The mode shapes shown are for maximum amplitude from the undeformed position. As can be seen, the motion is mostly at the tip. The motion appears to change from bending to bending/torsion coupling as the rotor speed is increased. The shapes of four different vibration modes are shown in Fig. 8 assuming an operating speed of 7500 rpm. These shapes indicate coupled motion.

The coupled motion is better illustrated by the effects of rotor speed on the nodal line shifting, as shown in Fig. 9 for the first vibration mode. The nodal line shifts slowly initially and then dramatically as the rotor speed is increased. The vibration mode up to 6000 rpm is predominately bending. However, it changes to torsional at 9000 rpm. It may be going through a "jumping" phenomenon at 7500 rpm, as shown by the single node point at the leading edge near the tip, prior to changing to the torsional mode. The nodal lines for the four different modes at 7500 rpm are shown in Fig. 10. These nodal lines indicate the coupled vibration motion of 60 deg swept turboprops. The coupled vibration motion is mostly at the tip and includes some chordwise modes. The coupled vibration modes and the progressive shifting of the nodal lines

Table 2 Summary of frequencies for swept titanium turboprop

Rotor speed, rpm	Frequency, Hz, for vibration mode 1	2	3	4
0	101.6	235.0	485.0	554.2
2500	117.1	241.7	487.7	571.2
5000	151.6	255.0	491.2	618.6
6500	174.1	261.6	488.7	655.8
7500	187.6	265.2	486.1	680.8
9000	200.0	270.5	475.0	711.2

NOTE: Frequencies predicted using COBSTRAN.

Table 3 Summary of frequencies for swept composite turboprop

Rotor speed, rpm	Frequency, Hz, for vibration mode 1	2	3	4
0	149.3	295.2	589.0	653.1
3000	161.8	295.5	585.7	678.4
4500	174.1	295.3	580.8	708.7
6000	185.2	294.7	572.8	748.6
7500	188.0	295.6	561.1	795.4
9000	169.4	301.4	544.6	843.5

NOTE: Frequencies predicted using COBSTRAN.

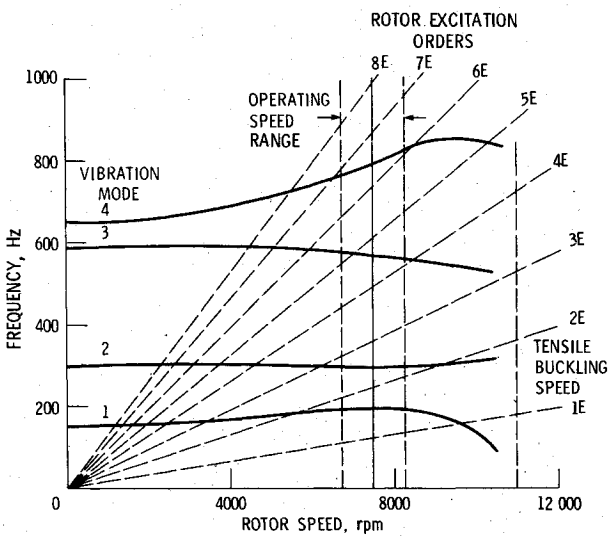

Fig. 6 Campbell diagram with rotor excitations.

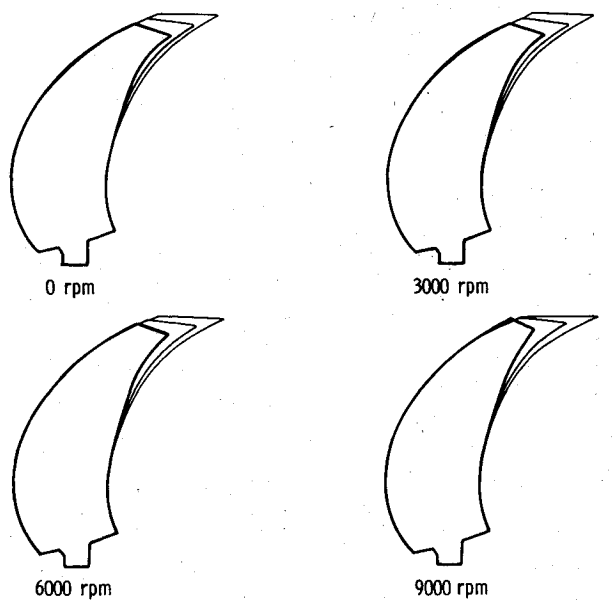

Fig. 7 Mode 1 vibrations of a 60 deg swept composite turboprop at various rotor speeds.

with increasing rotor speed make it highly questionable whether the dynamic response and flutter of swept turboprops can be assessed using beam modes or even finite element predicted modes at zero rotor speed.

Geometric and Material Coupling

The angle of sweep, the angle of twist, and the stacking on the helix induce geometric coupling in the presence of a centrifugal force field. This coupling can be easily assessed by examining the stiffness matrix at a node, preferably at the tip. Normalized stiffness matrices for the 60 deg swept titanium and composite turboprops are summarized in Table 4. These stiffness matrices were determined by applying successively a unit displacement in each direction at the tip midchord node while keeping the other five displacements fixed. The degree of geometric coupling is indicated by the off-diagonal terms that couple, for example, the radial displacement u to the other two forces (F_y and F_z) and to the three moments (M_x, M_y, M_z). Note that the coupling of the three moments to the displacements (u,v, and w) is substantial. Note also the substantial coupling between the in-plane moment M_z and out-of-plane moment M_y. These couplings are consistent with previous comments relative to Eqs. (6) and (7). The presence of these couplings make it necessary to use nonlinear finite element analysis[1] to realistically evaluate the structural response of swept, twisted turboprops.

Swept, twisted composite turboprops may also exhibit material coupling in addition to the geometric coupling just discussed. Material coupling in composites is present in either unsymmetric and/or unbalanced laminate configurations.[7] An indication of material coupling is obtained by comparing corresponding coefficients of the normalized stiffness matrices for the titanium and composite turboprops in Table 4. Comparing corresponding coefficients, it is seen that 1) the composite turboprop has greater in-plane coupling (F_x with v and w, for example) than the titanium turboprop; and 2) both turboprops have about the same in-plane (membrane)/bending coupling (F_x with θ_x, θ_y, and θ_z, for example) and also about the same bending twisting coupling (M_x with θ_y and θ_z). The greater in-plane coupling (F_x with w and u) is expected because of the greater Poisson's ratios of the (0 ± 45)

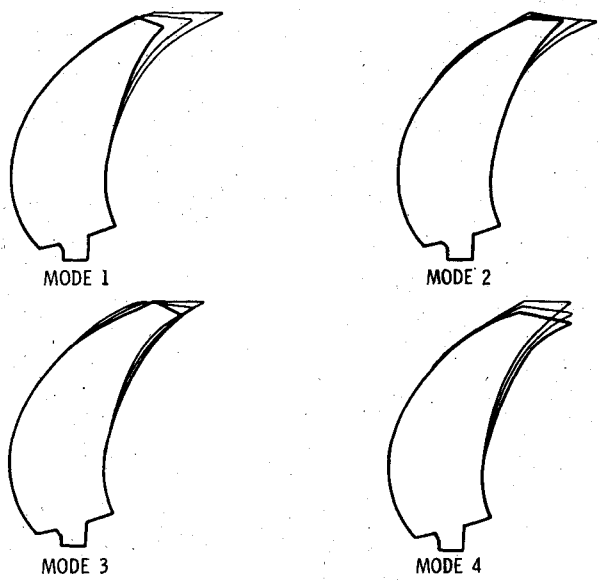

Fig. 8 Vibration modes of a 60 deg swept composite turbobrop at 7500 rpm rotor speed.

Table 4 Normalized stiffness matrices at tip midchord (60 deg swept turboprops)

Titanium

$$\begin{Bmatrix} F_x \\ F_z \\ F_y \\ M_x \\ M_z \\ M_y \end{Bmatrix} = \begin{bmatrix} 1.00 & 0.41 & 0.44 & 0.07 & -0.08 & -0.030 \\ & 0.37 & 0.27 & 0.07 & -0.04 & -0.006 \\ & & 0.24 & 0.04 & -0.03 & -0.008 \\ & & & 0.06 & -0.03 & -0.001 \\ & \text{Symmetric} & & & 0.03 & 0.012 \\ & & & & & 0.008 \end{bmatrix} \begin{Bmatrix} u \\ w \\ v \\ \theta_x \\ \theta_z \\ \theta_y \end{Bmatrix}$$

Composite

$$\begin{Bmatrix} F_x \\ F_z \\ F_y \\ M_x \\ M_z \\ M_y \end{Bmatrix} = \begin{bmatrix} 1.00 & 0.53 & 0.50 & 0.09 & -0.08 & -0.025 \\ & 0.49 & 0.36 & 0.07 & -0.05 & -0.007 \\ & & 0.30 & 0.05 & -0.03 & -0.008 \\ & & & 0.06 & -0.03 & 0.004 \\ & \text{Symmetric} & & & 0.03 & 0.011 \\ & & & & & 0.006 \end{bmatrix} \begin{Bmatrix} u \\ w \\ v \\ \theta_x \\ \theta_z \\ \theta_y \end{Bmatrix}$$

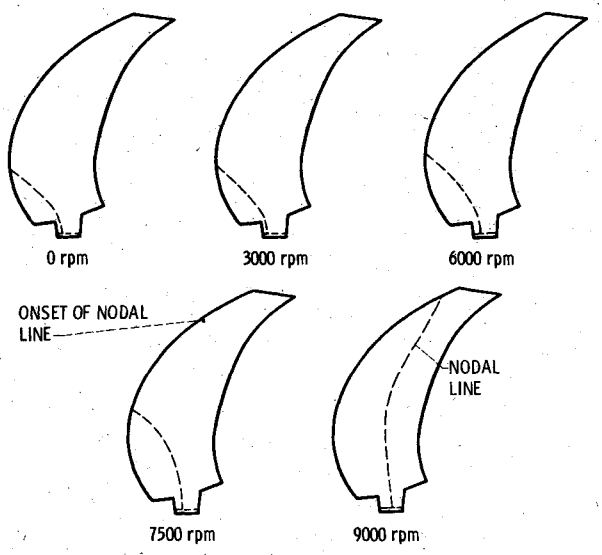

Fig. 9 Effects of rotor speed on the vibration model 1 nodal lines, 60 deg swept composite turboprop.

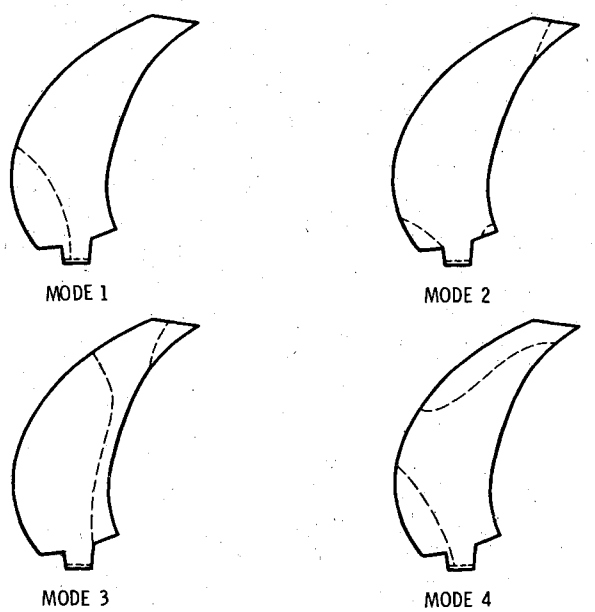

Fig. 10 Nodal lines of vibration modes, 60 deg swept composite turboprop at 7500 rpm rotor speed.

composite compared to titanium. Otherwise, the turboprops are similar and differ only in density (0.16 lb/in.^{3} for titanium, 0.057 lb/in.^{3} for composite). The weights for the two simulated turboprops are: 0.70 lb for the titanium and 0.25 lb for the composite. One point worth noting is that the frequency improvements of the composite turboprop relative to the titanium (Tables 2 and 3) are due mostly to the lighter density of the composite materials.

The previous discussion was only for turboprops with 60 deg sweep angles. However, the collective steps of the method used constitute a structured procedure. This procedure can readily be used to study the effects of sweep angle on tensile buckling rotor speeds and the attendant structural responses. The procedure can also be used investigate other aspects such as delamination due to through-the-thickness shear force, higher tensile buckling modes, and estimates on flutter.[8]

Summary

The significant results of an investigation on the tensile buckling of swept advanced propeller blades (turboprops) are as follows:

1) Tensile buckling has negligible effects on vibration frequencies when the rotor speed is less than 80% of the tensile buckling speed.

2) Tensile buckling occurs in swept turboprops because the centrifugal force field induces substantial in-plane compressive forces at the hump.

3) Composite turboprops have a possible advantage (about 130%) over titanium on a tensile buckling speed-to-weight basis. However, the titanium turboprops have about 15% greater tensile buckling speed.

4) Increased shear stiffness has negligible effect on the tensile buckling speed of composite turboprops.

5) The buckled mode shapes are primarily tip modes, are extensively coupled, and exhibit substantial tip motion, including some chordwise modes.

6) The vibration mode nodal lines shift with increasing rotor speed, indicating dramatic changes in the vibration mode shapes.

7) Substantial geometric coupling is present in both turboprops, but no material coupling exists in the symmetric composite, other than that due to Poisson's effect.

References

[1]Aiello, R. A. and Chamis, C. C., "Large Displacement and Stability Analysis of Nonlinear Propeller Structures," NASA TM-82850, 1982.

[2]Timoshenko, S. P. and Gere, J. M., *Theory of Elastic Stability*, 2nd ed., McGraw-Hill Book Co., New York, 1961, pp. 373-379.

[3]Lekhnitskii, S. G., *Anisotropic Plates*, Gordon and Breach, New York, 1968, pp. 459-465.

[4]Chamis, C. C., "Integrated Analysis for Engine Structures," NASA TM-82713, 1981.

[5]McNeal, R. H., "The NASTRAN Theoretical Manual (Level 15.0)," NASA SP-221(01), 1972, Sec. 7.

[6]Timoshenko, S., Young, D. H., and Weaver, W. Jr., *Vibration Problems in Engineering*, 4th ed., John Wiley & Sons, New York, 1974.

[7]Chamis, C. C., "Computer Code for the Analysis of Multilayered Fiber Composites-User's Manual," NASA TN D-7013, 1971.

[8]Chamis, C. C. and Aiello, R. A., "Tensile Buckling of Advanced Turboprops," NASA TM-82896, 1982.